Approaching the theoretical depairing current in $YBa_2Cu_3O_{7-x}$ nanowires

S.Nawaz[a], R.Arpaia[a,b,*], T.Bauch[a], F.Lombardi[a]

[a] *Quantum Device Physics Laboratory, Department of Microtechnology and Nanoscience, Chalmers University of Technology, SE-41296 Göteborg, Sweden*
[b] *CNR-SPIN, Dipartimento di Scienze Fisiche, Università degli Studi di Napoli Federico II, I-80126 Napoli, Italy*

Abstract

$YBa_2Cu_3O_{7-x}$ nanowires, with lateral dimensions smaller that 50 nm have been fabricated by a soft etching procedure preserving an Au capping layer on top of the nanostructure. We have obtained YBCO nanowires carrying critical current densities J_c close to the theoretical depairing limit. The resistive transition and the J_c as a function of temperature of the Au capped nanostructures have been compared with those where the Au protective layer was subsequently removed. We conclude that the Au capping layer together with the soft etching procedure are instrumental in preserving *pristine* superconducting properties very close to the as grown film. Our results open new perspective for the use of YBCO nanostructures in fundamental studies aiming at shedding light on the mechanism for high critical temperature superconductivity.

Keywords: high-temperature superconductors, nanofabrication, phase slips

In the recent years there has been great attention towards the study

*Corresponding author
Email address: riccardo.arpaia@chalmers.se (R.Arpaia)

of the superconducting phenomenon at the nanoscale. The motivation was driven by two contrasted interests: to understand the enhancement of the superconducting properties in low dimensional structures like nanowires [1, 2] and nanodots [3, 4] and at the same to establish the critical size limit beyond which the superconducting phenomenon cannot be sustained [5, 6, 7]. The advances of the nanotechnologies applied to these materials have also made clear that nanoscale superconductivity can be instrumental to develop quantum limited sensors able to probe the physical properties of nano objects with unprecedented resolution [8, 9].

For definition, nanoscale superconductivity involves structures with dimensions smaller than the characteristic lengths of the material, namely the coherence length ξ and the London penetration depth λ_L. While this regime is readily achievable for conventional superconductors [7], it still represents a challenge for cuprates High critical Temperature Superconductors (HTS). The chemical instability of these materials, mostly related to oxygen out-diffusion, and the extreme sensitivity to defects and disorder due to very short ξ (of the order of 1 nm), do represent real issues in establishing reliable nanofabrication routines. The challenge here is to realize homogeneous HTS nanostructures preserving *pristine* superconducting properties. The possibility to fabricate, for example, HTS nanowires with properties close to the as-grown film, beyond the technological impact of the high critical temperature, can also be instrumental to test truly foundational properties of these unconventional superconductors where nanoscale ordering and phase transitions have a critical role in building up the unconventional ground state [10, 11]. Up to now the transport properties of HTS nanowires, available

in literature, present such a spread of values, that it is difficult to draw a clear picture of the physics in play [12, 13, 14, 15, 16]. Recent results indicate that the ultimate $YBa_2Cu_3O_{7-x}$ (YBCO) nanowire lateral size can go down to 10 nm in arrays of several micron length, but at the expenses of the superconductivity, strongly affected by the patterning procedure [17]. In this paper we demonstrate that by a careful tuning of the nanopatterning procedure we are able to get nanowires down to 40 nm in width and from 200 nm to several micron in lengths exhibiting a similar critical temperature of the electrodes (differing not more than 1 K) and carrying critical current densities J_c close to the theoretical depairing limit. This last point is an issue even for conventional superconductors [18], and it represents a measure of the highly uniform superconductive properties of our nanowires. Our structures can be therefore considered model system to study the *intrinsic* nanoscale properties of HTS. The wide range of lengths we have been able to achieve also allows to span a broad range of applications going from nanoSQUIDs [8] for the shortest wires to single photon detectors for the longest one [19].

The wires were fabricated by depositing a 50 nm thick film of YBCO on a (110) MgO substrate by Pulsed Laser Deposition (PLD). The growth conditions were optimized to get the right compromise between surface smoothness and critical temperature T_c. We have gotten epitaxial thin films with a T_c of $\sim$ 85 K and a rather sharp transition (with width below 1 K) and an average surface roughness below 2 nm measured by Atomic Force Microscopy (AFM). For comparison we have also fabricated nanowires from commercial YBCO films grown on (001) MgO substrates, purchased from Theva. These films have surface morphology and structure properties comparable with those

grown in our laboratory and only slightly higher transition temperature (1-2 K).

A 200 nm thick layer of Au was immediately deposited after the deposition of the YBCO film to avoid any oxygen loss and other contaminations. The Au bonding pads were then defined by conventional photolithography and Ar^+ ion etching bearing in mind to preserve a 50 nm think Au film acting as a cap layer on the remaining YBCO. For the definition of the nanowires we have used a 100 nm thick amorphous carbon film working as a hard mask [14] in combination with electron beam lithography and Ar^+ ions etching. This last step is rather crucial: the interaction of Ar^+ ions with the YBCO film can cause drastic changes in film stoichiometry and disorder strongly affecting the transport properties. This effect becomes even more crucial if one is dealing with nanostructures, like nanowires. Severe differences can be observed in the transport properties, in particular the critical current density value and its temperature dependence, by tiny variations in the Ar^+ ion etching routines. A good control on the etching of YBCO nanowires is essential to get reproducible results at the nanoscale. This can be achieved by tuning the etching parameters to avoid overheating of the samples, and by carefully calibrating the etching time to minimize the interaction of Ar^+ ions with the nanowires. We have chosen to work close to the threshold beam voltage value V_{beam} for YBCO, which is of the order of 300 V. Below this value we have observed that the film is not etched. Moreover we have used the lowest beam current $I_{beam} = 5$ mA which allowed the ignition of a stable plasma in our milling system and we have worked with the neutralizer current off to avoid possible radiation heating coming from the neutralizer filament.

To summarize, by using the etching parameters $V_{beam} = 300$ V, $I_{beam} = 5$ mA and $J = 0.08$ mA/cm^2 with J being the density of current of the Ar^+ ions impinging on our sample, the nanowires are etched in roughly 2 h (this time also includes a 50 nm etching into the substrate). Here we present the electric transport properties of YBCO nanowires as a function of the lateral width obtained by using three different nanopatterning procedures: a) A 50 nm thick Au layer is kept on top of the YBCO nanowires b) The Au cap layer is completely etched calibrating the procedure so as to stop right at the complete removal of the Au (optimally etched samples) c) The surface of the wire is slightly etched after the capping Au is completely removed (overetched samples). In this case, we have calibrated the procedure so as a thickness of YBCO between 3-5 nm is removed from the nanostructures.

All the samples presented here have been etched with the same Ar^+ beam parameters. Fig. 1 shows a scanning electron microscope image of our narrowest wires 200 nm (Figs. 1(a) and 1(b)) and 3 μm (Figs. 1(c) and 1(d)) long, respectively. In all cases, to extract the effective dimensions of the nanostructures, we have used both Atomic Force Microscopy (AFM) and Scanning Electron Microscopy (SEM). The transport properties of the nanowires were obtained by conventional four point measurement in a ^{3}He refrigerator reaching a base temperature of 300 mK. More than 200 nanowires, varying in width from 40 nm to 2 μm and length from 200 nm to 3 μm, have been measured. Fig. 2(a) shows the critical current density J_c, as a function of the width, for a fixed length of 200 nm, for three different nanopatterning regimes a), b) and c). The plotted values of critical current densities, for the various nanopatterning procedures, refer to nanowires belonging to a single

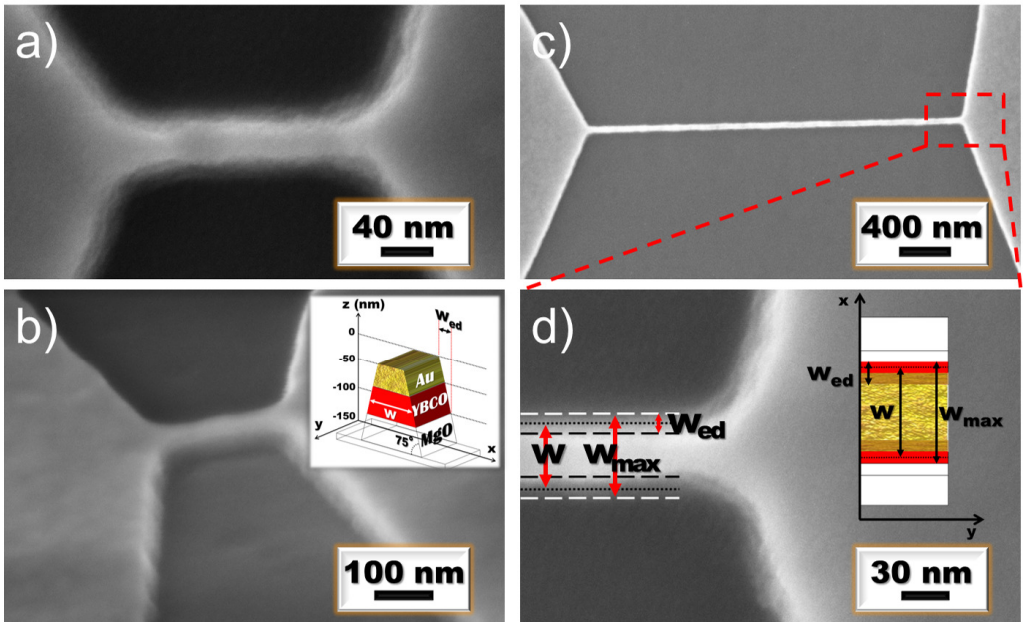

Figure 1: a) SEM picture of a 40 nm wide Au capped YBCO wire. The same nanowire with a 45° tilt angle of the SEM stage is shown in b). These pictures highlight the different boundaries Au/YBCO and YBCO/substrate. The inset in panel b) is the schematics of an AFM cross section, from which we can determine the slope and the width w_{ed} of the side walls (respectively $\sim 75°$ and ~ 25 nm) and confirm the 50 nm overetching into the substrate, used to avoid redeposition of YBCO in the vicinity of the nanowire. The width of the bridge, w, is defined as the bridge width at half the YBCO film thickness. c) SEM pictures of a Au capped 3 μm long wire, shown with higher magnification in d) so to confirm the uniformity of the nano structure. The inset in d), top view of the AFM cross section, shows the wire from the SEM perspective: the w_{ed} determined from the SEM picture is in good agreement with the one we estimate from the AFM. Thence, we determine the width of a bridge from SEM, $w = w_{max} - \frac{w_{ed}}{2}$, where w_{max} is the width of the bridge at the interface between YBCO and MgO.

chip. The red symbols refer to nanowires, with a 50 nm Au capping layer, patterned on a (110) MgO substrate (circles) and (001) MgO substrate (triangle) (procedure a). We observe two important features: 1) a monotonic increase of J_c with decreasing width w. This is found even for w values smaller than the Pearl length, $\lambda_P = \lambda_L^2/t$ that in our case is of the order of 1 μm (for a thickness $t = 50$ nm and $\lambda_{ab} \approx 200$ nm) and 2) the smallest wires have a J_c larger than 10^8 A/cm^2. The wires obtained by procedure b) (optimally etched samples) show almost the same behavior as the ones with an Au capping layer with only slightly smaller values of J_c for all widths (Fig. 2(a), blue diamonds). The situation dramatically changes for the structures obtained with procedure c) (overetched samples, black squares). Here the J_c is severely reduced for width below 100 nm. The degradation of the superconductive properties by reducing the width of the nanowire has been previously reported by many authors [12] (also see the references therein). Now we uniquely demonstrate that it is due to a prolonged interaction of the YBCO nanostructure with the milling species, almost vertically impinging the surface of the nanobridges and possibly causing drastic changes in the film stoichiometry and disorder. The record J_c values achieved in our experiments, by keeping the Au capping on the nanobridges, can be therefore attributed to the extremely gentle and slow etching process, never used earlier to fabricate YBCO nanostructures, and to the capping layer preventing the interaction between the Ar^+ ions and the surface of the nanobridge. To assess the criticality of the capping layer we have made control experiments by changing the thickness of the Au protective film. By reducing the Au thickness to 30 nm we got for $w < 150$ nm J_c values about $30 \div 40\%$ lower

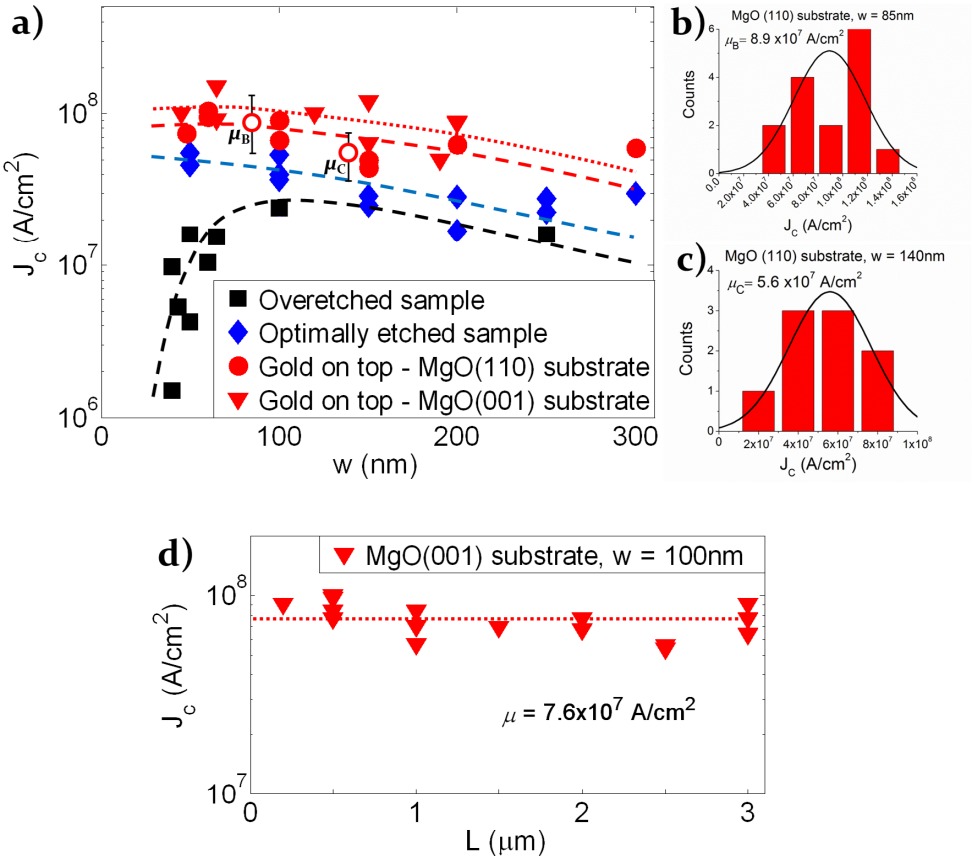

Figure 2: a) Width dependence of the critical current density J_c at T=4.2 K for 200 nm long YBCO wires with and without a Au capping layer. The dashed lines are guides for the eyes. The two open red circles represent the mean values (together with their standard deviations) of the J_c distributions of two sets of nanowires with fixed width w = 85 nm (panel b) and w = 140 nm (panel c). d) J_c dependence on length, in the range 200 nm - 3 μm, for 100 nm wide nanowires, patterned on the same chip. The dashed line is the mean value of the J_c distribution for these nanowires.

with respect to the red triangles and red circles of Fig. 2(a). On the other hand a thicker Au coverage, of the order of 100 nm, put limits to the minimum achievable lateral size of the nanowires: widths $w < 80-100$ nm cannot be achieved because of the erosion of the C mask caused by longer ething times.

The increasing of J_c by reducing the width (Fig. 2(a), red and blue points) of the nanowires is opposite to what has been published in literature up to now. In ref. [16] the authors find a steady reduction of the J_c from $w \sim 1$ μm till 200 nm with values never exceeding 10^7 A/cm^2 at 4.2 K. An almost constant J_c for nanowires in the range 50 nm $\leq w <$ 150 nm has been obtained in ref. [14]. However in this case the maximum achieved J_c was of the order of 10^6 A/cm^2. More recently Xu et al. have succeeded in fabricating parallel arrays of hundreds of YBCO nanowires with widths down to 10 nm and lengths of several microns. The average J_c of a single wire was as low as 10^5 A/cm^2 for $w = 15$ nm with a transition temperature below 20 K. In the attempt to improve the superconducting properties of YBCO nanowires, Papari et al. have made preliminary studies of the role of a protecting layer of Au. They have obtained substantial improvement in the performances for nanowires widths $\approx$ 150 nm with J_c as high as $7 \cdot 10^7$ A/cm^2. However for narrower wires they still observed a decreasing J_c by reducing the wire's width with values not exceeding $2 \cdot 10^7$ A/cm^2 for 50 nm wide wires. More importantly in their work the narrower nanowires showed a transition temperature several degrees lower compared to the larger one. This indicates significant damages at the smallest nanowire widths, possibly due to a too thin Au protecting layer of only 20 nm and to a non-optimal

Ar^+ ion etching parameters for very narrow wires.

To strengthen the finding that our J_c is increasing by reducing the nanowire width, we have realized 2 samples with the procedure "Gold on top, MgO (110) substrate" where only nanowires with fixed width 85 nm and 140 nm respectively were patterned. The idea was to get on the same chip the statistic of the distribution of the J_c values for a specific nanowires width. Fig. 2(b) shows the distribution of values for $w = 85$ nm while Fig. 2(c) for $w = 140$ nm. The mean values μ_B and μ_C together with the standard deviation are shown in Fig. 2(a) (open circles). These average values agree extremely well with the expected ones for those widths, further strenghtening the point that the J_c values reported in Fig. 2(a) are representative of a specific width. In Fig. 2(d) we show the critical current density measured at 4.2 K for 100 nm wide bridges as a function of bridge length (from 200 nm to 3 μm). The independence on length of the critical current density rules out any kind of artifact, in the determination of our very high values of J_c, due to possible redeposition of YBCO in the vicinity of the bridges.

Within the Ginburg-Landau (GL) theory the expression of the depairing current density is given by [20]:

$$j_d^{GL} = \frac{\phi_0}{3^{3/2}\pi\mu_0\lambda^2(T)\xi(T)} \tag{1}$$

where ϕ_0 is the flux quantum and μ_0 the vacuum permeability. In the limit of low temperature, the typical values for the penetration depth and coherence length for (001) YBCO films with a T_c of 85 K are $\lambda_{ab}(0) = 150 - 250$ nm and $\xi_{ab}(0) = 1.4 - 2$ nm respectively [12, 21, 22, 23]. These values give a depairing current density of about $J_d^{GL} \sim 1 - 3 \times 10^8$ A/cm^2, which is very close to that of the smallest wires fabricated with procedure a) and b). By

carefully tuning the etching parameters we have been able to get critical current densities approaching the depairing limit which proves we engineer *pristine* YBCO nanowires that are retaining the properties of the as-grown films. The fact that we observe an increased J_c for nanowires with $w << \lambda_P$ is somewhat unexpected; for an infinite long wire a saturation of J_c (reaching the theoretical depairing value) is obtained already for width $w \sim \lambda_P$, since the Pearl length represents the typical length scale on which the current density can vary [24]. The discrepancy between the experimental data and the expected behavior for infinite long wires, however, can be explained by taking into account the influence of the on-chip (wide) electrodes connecting the wire to the bias circuitry (see Fig. 1(b)). In this case, as it has been demonstrated in [24, 25], the current injection from the wide electrodes into the thin wire causes current crowding at the inner corners of the junction between wire and electrode, i.e. the local current density at the inner corners is enhanced compared to the average current density at the center of the wire. This causes that the current density at the corner can reach the depairing current density limit while in the center of the wire the current density is still below that limit. As a consequence the average J_c of the wire is below the J_d^{GL} even for wires with $w << \lambda_P$ [25].

To further demonstrate the excellent quality of the nanowires, in terms of uniformity of the transport properties, we have measured the critical current density as a function of the temperature J_c(T) for more than 100 nanostructures. For low critical temperature superconductor nanowires [26, 27] the dependence of the J_c(T) can be well interpolated, in the full temperature

range below T_c, by the Bardeen formula [28]

$$J_c\left(T\right) \propto \left(1-\left(T/Tc\right)^2\right)^{3/2} \tag{2}$$

In the case of HTS nano-structures various J_c(T) dependences are reported in literature and attributed to various mechanisms [29, 30]. Fig. 3(b) shows

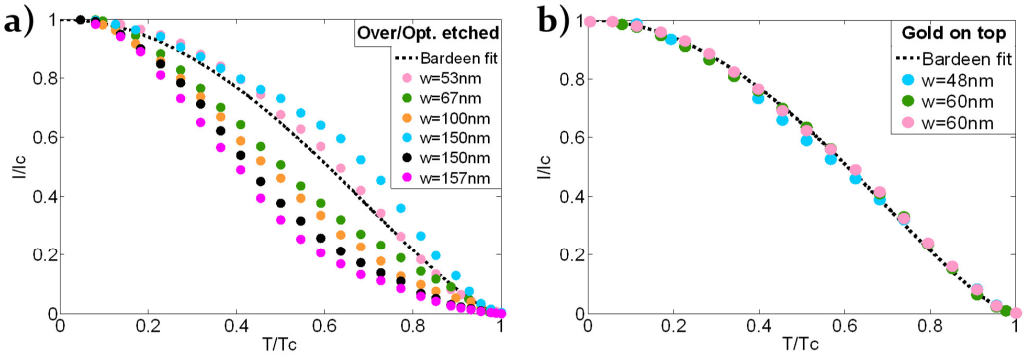

Figure 3: Normalized critical current as a function of temperature for (a) overetched and optimally etched nanowires, and (b) nanowires with a gold capping layer.

a plot of J_c(T) for some of our narrowest ($w \leq 60$ nm) wires covered with Au. For all widths, the normalized J_c(T) follows nicely the Bardeen expression (2). This has been verified for more than 20 wires with a Au capping layer. This behavior drastically changes for the wires fabricated with procedures b) and c) as shown in Fig. 3(a). The normalized J_c(T), for the optimally etched and over-etched nanowires shows considerable from the Bardeen expression, with values in temperature both below and above the expected ones. Occasionally some of the optimally etched devices had a J_c(T) following the Bardeen formula probably indicating less damaged structures.

To assess the effect of the capping layer on the superconducting properties, we have analyzed and compared the resistance versus temperature measurements, R(T), for a nanowire with Au capping and for the same nanowire after removal of the Au capping (see Fig. 4). The current and voltage probes of our 4-point measurement setup are situated at the far ends of the two wide electrodes connected to our nanowires. Therefore we measure the resistance

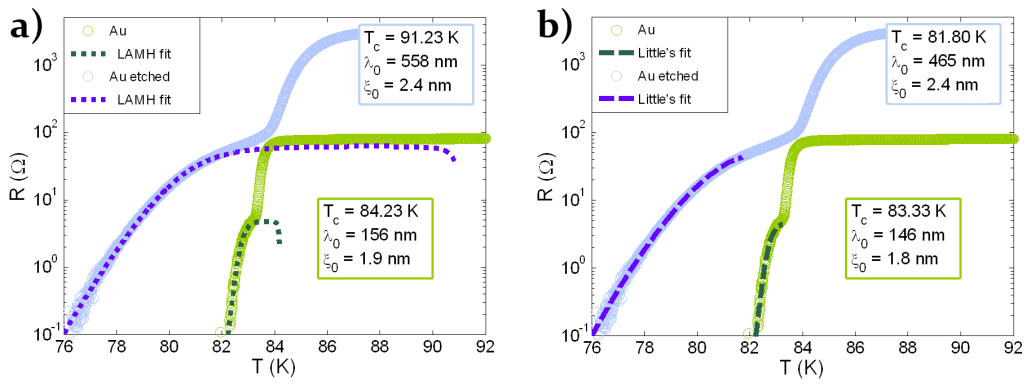

Figure 4: (a) Resistance as a function of temperature of a 200 nm long and 43 nm wide Au-capped nanowire (green circles) and of the same nanowire after the removal of the Au capping layer (blue circles). The used substrate is MgO (001). From the resistance at the onset temperature of the superconducting transition of the uncapped nanowire we can estimate the resistivity of the YBCO wire, $\rho_{YBCO,w} \sim 10^{-6}\Omega$m. The blue and green dashed lines are LAMH fits using equation 4 and equation 5, respectively. (b) The same two curves modeled with Little's fits (equations 6 and 7 for the wire before and after the removal of gold, respectively).

of the nanowire in series with the resistance of the two wide electrodes. On cooling the sample we first observe (see Fig. 4) the onset of the superconducting transition of the electrodes around T = 86 K (without Au capping)

and T = 84 K (with Au capping). Here it is important to note that the different onset temperatures are related to the additional resistive shunt of the Au film and are not due to a change of the superconducting transition temperature of the film [27]. Once the resistance of the electrodes drops below the normal resistance of the nanowire we can observe the superconducting transition of the wire, which is typically 1 K below the value of the wide electrodes.[1] Comparing the superconducting transitions of the wire capped with Au and the wire after the removal of Au we observe that the transition of the uncapped wire is much broader in temperature. In the following we will analyze the resistance as a function of temperature considering that thermally activated phase slip events are the dominating source of resistance during the superconducting transition. Following the Langer-Ambegaokar-McCumber-Halperin (LAMH) theory [31, 32] the finite resistance related to phase-slip processes R_{LAMH} writes as

$$R_{LAMH}(T) = \left(\frac{h}{4e^2}\right)\left(\frac{\hbar\Omega_D}{k_B T}\right) exp\left(-\frac{\Delta F}{k_B T}\right), \tag{3}$$

where $\Omega_D = (L/\xi)\sqrt{(\Delta F/k_B T)}\tau_{GL}^{-1}$ is the attempt frequency, k_B is the Boltzmann constant, L is the length of the wire, $\Delta F = \left(8\sqrt{2}/3\right)(B_c^2/2\mu_0)\,A\xi$ is the energy barrier for phase slip nucleation in a volume given by the cross sectional area of the wire, A, times the coherence length ξ, $\tau_{GL} = \pi\hbar/8k_B(T_c^w - T)$ is the relaxation time. Close to T_c^w, the coherence length ξ and critical field B_c are given by $\xi(T) = \xi_0(1 - T/T_c^w)^{-1/2}$ and $B_c(T) = B_c^0(1 - T/T_c^w)$, where $B_c^0 = \frac{h}{2e\sqrt{8}\pi\lambda_0\xi_0}$ is the thermodynamical critical field, λ_0 and ξ_0 are

[1] The T_c of the wires are independent of the width indicating that also the narrowest one (w $\sim$ 40 nm) has a T_c differing at most 1 K from that of the grown film.

the London penetration depth and the coherence length at $T = 0$ K, respectively. The total resistance of nanowires without Au capping layer close to the transition can be expressed as the parallel combination of R_{LAMH} and the normal resistance of the wire R_N [33]:

$$R(T) = \left(R_{LAMH}^{-1}(T) + R_N^{-1}\right)^{-1} \tag{4}$$

In the case of nanowires with a gold capping layer the gold film on top of the nanowire structures additionally shunts the YBCO nanowire:

$$R(T) = \left(R_{LAMH}^{-1}(T) + R_N^{-1} + R_{sh}^{-1}\right)^{-1} \tag{5}$$

where R_{sh} is the shunt resistance associated with the gold film. Our nanowires, in the temperature range where the transition takes place, are quasi-2D structures with a ratio $w/\xi \sim 4$. By considering the temperature dependence for the coherence lenght, and assuming a ξ_0 of 2 nm, typical for cuprates, we get that $\xi(T \approx 83$ K) is 15 nm. We can therefore use the LAMH theory that, although it is strictly valid for 1-dimentional systems ($w < \xi$), it has been proven to give reasonable results also in the case of two-dimensional objects [34].

In order to understand the local extension of the shunt resistance, R_{sh}, and to obtain an estimate of its value we numerically calculated the current distribution in a typical nanostructure (nanowire connected to two wide electrodes) for various values of the YBCO wire resistivity, $\rho_{YBCO,w}$. Here we used values for $\rho_{YBCO,w}$ from 10^{-6} Ωm, a value typical for our nanowires at the onset of the superconducting transition temperature (see Fig. 4), to 10^{-9} Ωm. For all calculations we used the same two boundary conditions: 1) the current is injected into the YBCO film at the far end of one electrode

and drained from the YBCO film at the far end of the other electrode and 2) the voltage difference between the two ends of the electrodes is kept at a fixed value. In the calculations we neglected the proximity effect between Au and YBCO and considered only a finite contact resistivity, $\tilde{\rho_c}$, between the gold and YBCO film. Moreover we assumed that the resistivity of the wide YBCO electrodes, $\rho_{YBCO,el}$, is much smaller than the resistivity of the Au film, ρ_{Au}, which is a reasonable approximation in the temperature range below which we can observe the superconducting transition of the Au-capped YBCO wire ($T_{onset,w} \approx 83$ K, see Fig. 4). Fig. 5(a) shows the logarithm of the local current density in a nanowire structure for the YBCO wire resistivity slightly below its normal state resistivity value, $\rho_{YBCO,w} = 4 \times 10^{-7}$ Ωm. The logarithm of the current density for $\rho_{YBCO,w} = 1 \times 10^{-8}$ Ωm, i.e. 100 times smaller than its normal state value, is shown in Fig. 5(b). One can clearly see that the current density inside the Au wire on top of the YBCO wire is approximately constant. The current redistribution between the Au and YBCO film occurs mainly within an area indicated by the two half circles inside the electrodes (indicated by the dotted lines in Fig. 5(a)). Thus, we can approximate the shunt resistance by the series combination of the Au resistance on top of the wire, $R_{Au,w} = \frac{\rho_{Au} L}{wt}$, and the resistance associated with the current redistribution from the gold capping layer into the (superconducting/low ohmic) YBCO electrodes, R_{el}, i.e. $R_{sh} = R_{Au,w} + R_{el}$. Moreover the area over which the current redistributes between the two films inside the electrodes is practically independent of the value of the YBCO wire resistivity. To confirm this fact we calculated the total resistance of nanowire structures for various values of the YBCO wire resistivity $\rho_{YBCO,w}$,

which are shown in Fig. 5(c) (open symbols). Indeed, the data can be nicely fitted to $R^{tot} = \rho^{-1}_{YBCO,w} + R^{-1}_{sh}$ (solid line), which is just the wire resistance in parallel with a constant shunt resistance [35]. For the material parameters used in the calculations shown in Fig. 5 we obtain for the shunt resistance $R_{sh} = R_{Au,w} + R_{el} = 4.3\ \Omega$, with $R_{Au,w} = 2.4\ \Omega$ and $R_{el} = 1.9\ \Omega$.

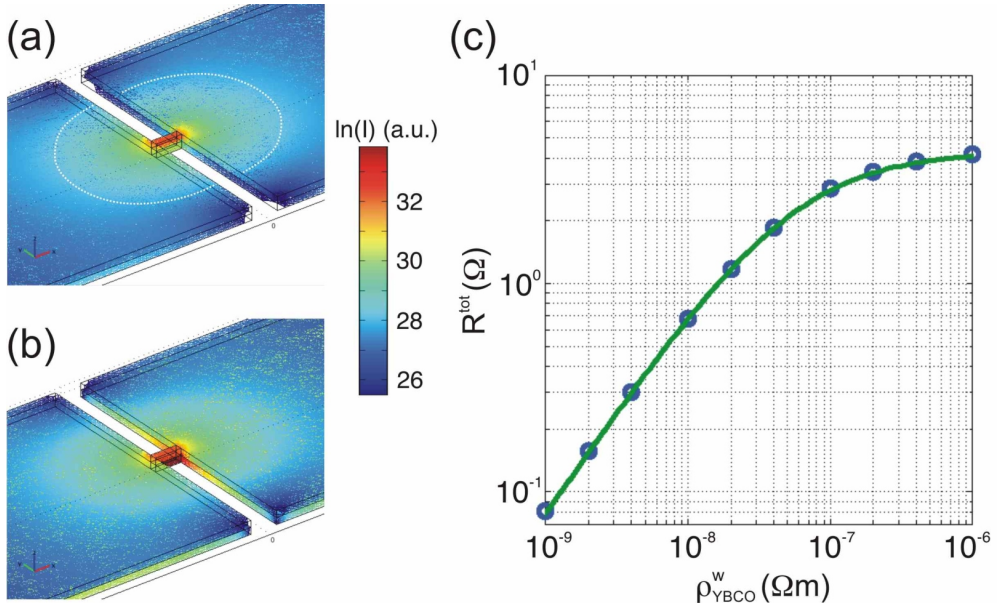

Figure 5: a)Numerical calculation of the current distribution in a nanowire structure. Both the bottom film (YBCO) and top film (Au) have a thickness of 50 nm. The wire has a length L = 200 nm and width w = 50 nm. The width of the electrodes is 2 μm. The following material parameters have been used: $\rho_{Au} = 3 \times 10^{-8}\Omega$m , $\rho_{YBCO,el} = 1 \times 10^{-11}\Omega$m, $\tilde{\rho_c} = 1 \times 10^{-12}\Omega m^2$, and $\rho_{YBCO,w} = 4 \times 10^{-7}\Omega$m (a), and $\rho_{YBCO,w} = 1 \times 10^{-8}\Omega$m (b). (c) Numerically calculated total resistance of the nanowire structure as a function the YBCO wire resistivity $\rho_{YBCO,w}$ (open symbols). The solid line represents the parallel combination of the bare YBCO wire resistance and the shunting resistance $R_{sh} = 4.3\ \Omega$. The contribution of the YBCO resistance in the electrodes is negligible.

Using equation 5 we can now fit the experimental R vs T of the nanowire with Au capping (dashed green line), obtaining the following fitting parameters: $\lambda_0 = 153$ nm, $\xi_0 = 1.9$ nm, and $T_c = 83.93$ K, which are typical values for YBCO thin films [21]. This further substantiates the pristine character of our nanowires. After removal of the Au capping layer, however, the fit to equation 4 provides unreasonable fitting parameters for the London penetration depth ($\lambda_0 = 554$ nm) and a T_c value ($T_c = 91.41$ K), which is above the superconducting transition temperature of the bare YBCO film. Therefore we can conclude that the thermal broadening most probably is not caused by thermal activation of phase slips. Instead, the very broad superconducting transition gives a strong indication that local damaging of the YBCO wire occurs during the removal of the Au capping layer. To further prove this statement, we have modeled the R vs T of our nanowires with the Little's fit [7]. This might be considered as a more accurate model describing the thermal activation of phase slips, since it avoids the intrinsic limitation of the LAMH model [7, 36, 37], where the presence in the pre-factor of the attempt frequency Ω_D, determining an unphysical zero resistance at the critical temperature, brings to an overestimation of the critical temperature of the wire. With the Little's fit, which has already been successfully applied to the description of the R vs T in LTS nanobridges [38], the resistance of the wire writes as [7]

$$R_{Little}(T) = R_N exp\left(-\frac{\Delta F}{k_B T}\right), \tag{6}$$

where the prefactor, differently from the LAMH fit, contains explicitely the normal resistance of the wire R_N. Similarly to eq. 5, in case the nanowire is covered by a gold capping layer acting as a shunt, the final resistance can be

expressed as:

$$R(T) = \left(R^{-1}_{Little}(T) + R^{-1}_{sh}\right)^{-1}. \quad (7)$$

We have fitted our uncapped and capped nanowires with eqs. 6 and 7 respectively (an example is shown in fig. 4(b)). For gold capped wires, we get a correct value for the critical temperature, with the London penetration depth and the coherence length values very similar to the ones extracted with the LAMH theory. Instead, when fitting the uncapped wires, the agreement with the data, once again, is achieved only by considering unfeasible values of the London penetration depths, much larger than those expected for YBCO. So, even though the Little's fit gives a correct critical temperature, the physics of the wires without a Au capping cannot be explained by considering thermal fluctuations.

In conclusion we have fabricated YBCO nanowires with cross sections as small as 40×50 nm^2 using three different fabrication procedures. We measured the critical current density as a function of temperature in a range between 300 mK and the superconducting transition temperature, T_c, and the resistance as a function of temperature close to T_c. From these measurements we can conclude that the wires with an Au capping layer preserve the superconducting properties of as grown films. For wires with the smallest cross sections we even obtain critical current densities of the order $10^8 A/cm^2$, a value very close to the depairing limit. Instead, the wires from which the Au capping layer was removed showed indications of degradation/damaging reflecting in non-reproducible J_c vs T behaviors and very broad superconducting transitions in R vs T measurements. These findings pave the way for new experiments exploring HTS superconductivity at the nanoscale [39].

Acknowledgement

This work has been partially supported by the Swedish Research Council (VR) and the Knut and Alice Wallenberg Foundation. Shahid Nawaz was partially supported by a grant from Higher Education Commission of Pakistan.

References

[1] A. A. Shanenko, M. D. Croitoru, M. Zgirski, F. M. Peeters, K. Arutyunov, Phys. Rev. B 74 (2006) 052502.

[2] F. M. Peeters, M. D. Croitoru, A. A. Shanenkor, Physica. C. 468 (2008) 326–330.

[3] S. Bose, A. M. Garcia-Garcia, J. D. Ugeda, M. M.and Urbina, C. H. Michaelis, I. Brihuega, K. Kern, Nature Materials 9 (2010) 550–554.

[4] A. M. Garcia-Garcia, J. D. Urbina, E. A. Yuzbashyan, K. Richter, B. L. Altshuler, Phys. Rev. Lett. 100 (2008) 187001–187004.

[5] N. Giordano, Phys. Rev. Lett. 61 (1988) 2137–2140.

[6] A. Bezryadin, C. N. Lau, M. Tinkham, Nature 404 (2000) 971–974.

[7] A. Bezryadin, J. Phys. Condens Matter 20 (2008) 043202–0432021.

[8] J. Gallop, Supercond. Sci. Technology 16 (2003) 1575–1582.

[9] J. Nagel, K. B. Konovalenko, M. Kemmler, M. Turad, R. Werner, E. Kleisz, S. Menzel, R. Klingeler, B. Büchner, R. Kleiner, D. Koelle, Supercond. Sci. Technology 24 (2011) 015015–015022.

[10] J. F. Ding, X. Q. Xiang, Y. Q. Zhang, H. Liu, X. G. Li, Phys. Rev. B 77 (2008) 214524–214529.

[11] Q. Li, M. Mucker, G. D. Gu, A. M. Tsvelik, J. M. Tranquada, Phys. Rev. Lett. 99 (2007) 067001–067004.

[12] G. Papari, F. Carillo, D. Stornaiuolo, L. Longobardi, F. Beltram, F. Tafuri, Supercond. Sci. Technology 25 (2012) 035011–035015.

[13] J. A. Bonetti, D. S. Caplan, D. J. Van Harlingen, M. B. Weissman, Phys. Rev. Lett. 93 (2008) 087002–087005.

[14] P. Larsson, B. Nilsson, Z. G. Ivanov, J. Vac. Sci. Technol. B 18 (2000) 25–31.

[15] J. Schneider, H. Kohlstedt, R. Wordenweber, Appl. Phys. Lett. 63 (1993) 2426–2428.

[16] H. Assink, A. J. M. Harg, C. M. Schep, N. Y. Chen, D. Marel, P. Hadley, E. W. J. M. Drift, J. E. Mooij, IEEE Trans. Appl. Supercond. 3 (1993) 2983–2985.

[17] K. Xu, J. R. Heath, Nano Lett. 8 (2008) 3845–3849.

[18] K. Xu, P. Cao, J. R. Heath, Nano Lett. 10 (2010) 4206–4210.

[19] H. Bartolf, A. Engel, A. Schilling, K. Il'in, M. Siegel, H.-W. Hübers, A. Semenov, Phys. Rev. B 81 (2010) 024502–024514.

[20] M. Tinkham, Introduction to Superconductivity, McGrahaw-Hill International Editions, New York, 2 edition, 1996.

[21] J. R. Waldram, Superconductivity of Metals and Cuprates, IOP publishing Ltd, Institute of Physics publishing Bristol and Philadelphia, 1996.

[22] Y. Zuev, M. S. Kim, T. R. Lemberger, Phys. Rev. Lett. 95 (2005) 137002–137006.

[23] K. Fossheim, A. Sudbø, Superconductivity: physics and applications, Wiley, New York, 2004.

[24] J. R. Clem, K. K. Berggren, Phys. Rev. B 84 (2011) 174510–174526.

[25] S. Nawaz, R. Arpaia, F. Lombardi, T. Bauch, Phys. Rev. Lett. 110 (2013) 167004.

[26] M. W. Brenner, S. Gopalakrishnan, J. Ku, T. J. McArdle, J. N. Eckstein, N. Shah, P. M. Goldbart, A. Bezryadin, Phys. Rev. B 83 (2011) 184503.

[27] M. W. Brenner, D. Roy, N. Shah, A. Bezryadin, Phy. Rev. B 85 (2012) 224507–224519.

[28] J. Bardeen, Rev. Mod. Phys. 34 (1962) 667–681.

[29] H. Darhamaoui, J. Jung, Phys. Rev. B 53 (1996) 14621–14630.

[30] A. L. Mansour, K. H. Chow, J. Jung, J. Appl. Phys. 110 (2011) 0639091–0639094.

[31] J. S. Langer, V. Ambegaokar, Phys. Rev. 164 (1967) 498–510.

[32] D. E. McCumber, B. I. Halperin, Phys. Rev. B 1 (1970) 1054–1070.

[33] R. S. Newbower, M. R. Beasley, M. Tinkham, Phys. Rev. B 5 (1972) 864–868.

[34] M. Bell, V. Mitin, J. Bird, A. Verevkin, G. Goltsman, Phy. Rev. B 76 (2007) 094521–094525.

[35] R. Arpaia, S. Nawaz, F. Lombardi, T. Bauch, IEEE Trans. Appl. Supercond. 23 (2013) 1101505.

[36] D. S. Golubev, A. D. Zaikin, Phys. Rev. B 78 (2008) 144502.

[37] D. Meidan, Y. Oreg, G. Refael, Phys. Rev. Lett. 98 (2007) 187001.

[38] S. L. Chu, A. T. Bollinger, A. Bezryadin, Phys. Rev. B 70 (2004) 214506.

[39] D. Gustafsson, D. Golubev, M. Fogelström, T. Claeson, S. Kubatkin, T. Bauch, F. Lombardi, Nature Nanotechnology 8 (2013) 25–30.